Proceedings of the Twenty-ninth (2019) International Ocean and Polar Engineering Conference **www.isope.org**
Honolulu, Hawaii, USA, June 16-21, 2019

ISBN 978-1 880653 85-2; ISSN 1098-6189

Numerical Approach in the Study of Tsunami-like Waves and Comparison with Experimental Data

Daisuke Nishiura[1], Davide Wüthrich[1,2], Mikito Furuichi[1], Shun Nomura[1], Michael Pfister[3], Giovanni De Cesare[2]
[1]Department of Mathematical Science and Advance Technology, Japan Agency for Marine-Earth Science and Technology (JAMSTEC), Yokohama, Japan
[2]Platform of Hydraulic Constructions, Ecole Polytechnique Fédérale de Lausanne (EPFL), Lausanne, Switzerland
[3]Civil Engineering Department, Haute Ecole d'Ingénierie et d'Architecture de Fribourg (HEIA-FR, HES-SO), Fribourg, Switzerland

ABSTRACT

A comprehensive understanding of physical phenomena based on a hybrid experimental-numerical approach supports a safer design of critical infrastructures. However, for large-scale tsunami-like waves, the reliability of numerical models was insufficiently validated. Herein, we validate our numerical model of tsunami-like waves by comparing simulation data (obtained using a smoothed particle hydrodynamics method based on a highly efficient parallel computing technique) with large-scale experimental data for both, dry bed surges and wet bed bores. The presented preliminary results are believed to aid the development of experimentally validated numerical tools for a better understanding of tsunami-like flows.

KEYWORDS: SPH simulation; tsunami; validation; wet bed; dry bed; dam-break; wave profile.

INTRODUCTION

Tsunamis, impulse waves, dam-break waves, and flood surges are rare but catastrophic events that incur human losses and damage infrastructure. At present, the observation and estimation of wave-induced loads remains challenging because of the complexity of the underlying processes. Despite the numerous studies carried out, a more accurate estimation of wave-induced loads is necessary for the design of safer infrastructures and reliable vertical shelters, which highlights the importance of hybrid experimental-numerical approaches for a comprehensive understanding of the associated physical phenomena.
Most studies performed on tsunami-like waves to date are based on an experimental approach (Lauber and Hager, 1998; Ramsden, 1993; Nouri et al., 2010). For example, the hydrodynamic properties of dam-break waves were shown to be similar to those of flows observed during extreme hydrodynamic events, i.e., these unsteady flows can be used to reproduce tsunami-like waves propagating inland (Chanson, 2006). Previous experimental studies conducted at the Laboratory of Hydraulic Constructions (LCH) at Ecole Polytechnique Fédérale de Lausanne (EPFL) in Switzerland present a technique allowing one to generate tsunami-like waves through the vertical release of a water volume from an upper reservoir into a lower channel (Wüthrich et al., 2016a, 2018). This technique was successfully compared to the dam-break scenario to simulate tsunami-like flows, and both dry bed surges and wet bed bores were generated because of installation flexibility, simulating the first and any subsequent wave of the tsunami propagating inland. Wave heights and velocity profiles were measured using seven ultrasonic distance sensors (USs) and one ultrasonic velocity profiler (UVP; Fig. 1), which allowed an in-depth investigation of the main hydrodynamic properties of tsunami-like flows to be carried out.

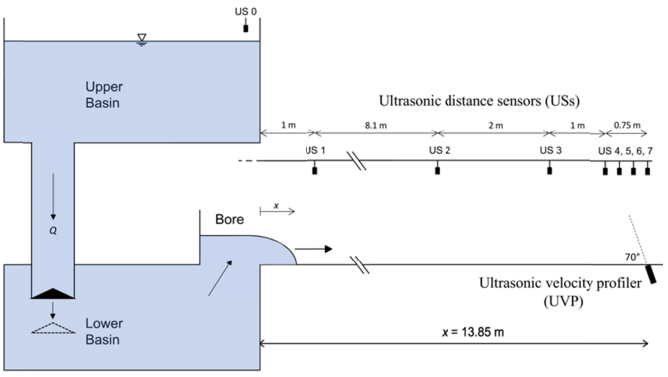

Fig. 1 Schematic of the vertical release channel and the location of instruments used in the experimental study conducted at LCH-EPFL.

In parallel, numerical simulation models allowing actual tsunami phenomena to be reproduced with high similarity and reproducibility may potentially be useful for the design of safer infrastructure and anti-tsunami inundation plans. However, to be suited for tsunami research, numerical models should be validated in terms of accuracy and reliability. At present, some numerical models based on computational fluid mechanics have been developed to investigate tsunami-like flows (St-Germain et al., 2014; Crespo et al., 2015; Guler et al., 2018). During

development, such models are generally validated through comparison with experimental results and analytical solutions. However, most of these comparisons have been carried out only for simple wave flows on a small scale, i.e., the reliability of numerical models has not been sufficiently validated for large-scale tsunami-like waves.

In view of the above, this work aimed to compare the results of selected experimental tests carried out at LCH-EPFL with those provided by a numerical model developed at the Japan Agency for Marine-Earth Science and Technology (JAMSTEC). The above numerical model employed smoothed particle hydrodynamics (SPH) (Monaghan, 1992), adopting the explicit time integration method with parallel computing algorithms using a dynamic load balancing technique (Nishiura et al., 2015; Furuichi and Nishiura, 2017) to simulate large-scale tsunami-like waves on dry and wet beds. In contrast to mesh-based methods, SPH is a particle-based method that can easily deal with free surface flows such as tsunami (Fig. 2). However, this advantage over mesh-based techniques comes at the cost of decreased computational accuracy, which highlights the importance of knowing the accuracy and limitations of the SPH simulation model for reproducing experimental tsunami-like flows.

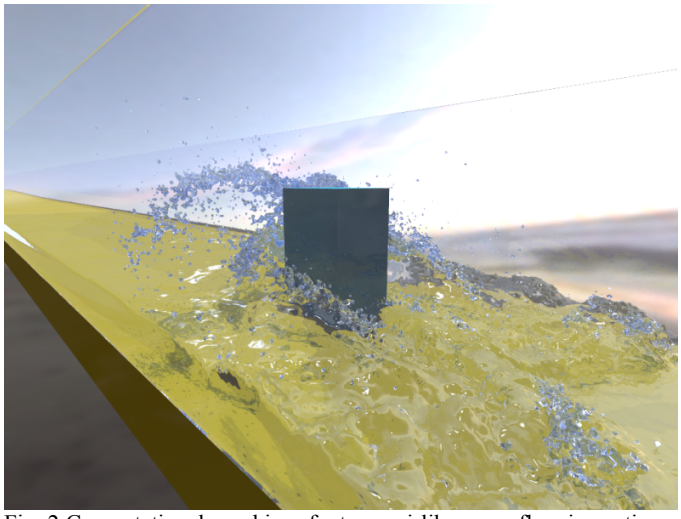

Fig. 2 Computational graphics of a tsunami-like wave flow impacting a structure obtained by large-scale SPH simulation corresponding to the LCH-EPFL experimental test.

At first sight, preliminary comparison of numerical simulations with large-scale experimental data reveals that these two approaches afford very similar results. Herein, the main hydrodynamic features (e.g., wave surface profiles, flow velocity distributions, and wave front celerities) of dry bed surges and wet bed bores are compared and discussed in more detail to obtain useful information on the reproducibility and limitations of experimentally validated numerical tools for a better understanding of tsunami-like flows. The gained insights are found to be potentially useful for estimating wave-induced loads on coastal structures.

NUMERICAL SIMULATION MODEL

Computational procedure used in the SPH method

Governing equations. SPH is a mesh-free simulation method that discretizes the fluid flow field with explicitly tracked reference particles (Monaghan, 1992). Each particle has a smooth kernel function characterized by spatial distance denoted as "smoothing length." In this research, Wendland's function was used as the kernel function W_{ij} with smoothing length l:

$$W_{ij} = \alpha_{\mathrm{D}} \left(1 - \frac{|\boldsymbol{r}_{ij}|}{2l}\right)^4 \left(\frac{2|\boldsymbol{r}_{ij}|}{l} + 1\right), \qquad 0 \le |\boldsymbol{r}_{ij}| \le 2l, \tag{1}$$

$$\boldsymbol{\nabla}_i W_{ij} = \alpha_{\mathrm{G}} \left(\frac{|\boldsymbol{r}_{ij}|}{2l} - 1\right)^3 \boldsymbol{r}_{ij}, \tag{2}$$

where $r_{ij} = r_i - r_j$ is the position of particle i relative to particle j, r_k denotes the position of particle k, and $\boldsymbol{\nabla}_i W_{ij}$ is the gradient of the kernel function. The coefficients of Eqs. (1) and (2) are different for two-dimensional (2D) and three-dimensional (3D) simulations, i.e., α_{D} equals $7/(4\pi l^2)$ and $21/(16\pi l^3)$ in 2D and 3D, respectively, while the respective expressions for α_{G} are given by $35/(4\pi l^4)$ and $105/(16\pi l^5)$.

Discretization of the Navier–Stokes equation of fluid with the kernel function allows the momentum and continuity equations to be expressed as

$$\frac{d\boldsymbol{v}_i}{dt} = -\sum_j m_j \left(\frac{P_j}{\rho_j^2} + \frac{P_i}{\rho_i^2}\right) \boldsymbol{\nabla}_i W_{ij} + \sum_j m_j \left(\frac{\nu_i + \nu_j}{\rho_i + \rho_j} \frac{2\boldsymbol{r}_{ij} \cdot \boldsymbol{\nabla}_i W_{ij}}{\boldsymbol{r}_{ij}^2 + \eta^2}\right) \boldsymbol{v}_{ij} \tag{3}$$

and

$$\frac{d\rho_i}{dt} = \sum_j m_j \boldsymbol{v}_{ij} \boldsymbol{\nabla}_i W_{ij}, \tag{4}$$

respectively, where $v_{ij} = v_i - v_j$ is the relative velocity of particle i relative to particle j, and v_k, P_k, ρ_k, ν_k, and m_k are the velocity, pressure, density, effective local viscosity, and mass of the k-th particle, respectively. η is a small parameter (set to $0.01l$) used for smoothing out the singularity at $r_{ij} = 0$. The local pressure in the first term on the right-hand side of Eq. (3) is given by the following equation of state, which is based on Tait's equation (Monaghan, 1994):

$$P_i = \frac{c_0^2 \rho_0}{\gamma} \left[\left(\frac{\rho_i}{\rho_0}\right)^{\gamma} - 1\right], \tag{5}$$

where $\gamma = 7$, ρ_0 is the reference density, and c_0 is the speed of sound at the reference density. Thus, in the above model, fluid is treated as weakly compressible. The second term on the right-hand side of Eq. (3) is the viscous stress force, while the right-hand side of Eq. (4) is compressibility (calculated by the kernel function).

The eddy viscosity effect caused by turbulence can be often incorporated into the viscos stress term using a large eddy simulation (LES) model. In this model, turbulence eddy viscosity is represented by the Smagorinsky mode:

$$\nu^{\mathrm{LES}} = (C_{\mathrm{s}}\Delta)^2 |S|, \tag{6}$$

where C_{s} is a constant most often equal to 0.17, S is the strain rate tensor, and Δ is the LES filter size (taken equal to the kernel smoothing length l in SPH). Therefore, the local effective viscosity ν can be expressed as a sum of kinematic viscosity ν^{K} and turbulence eddy viscosity:

$$\nu = \nu^{\mathrm{K}} + \nu^{\mathrm{LES}}. \tag{7}$$

Computational procedure. In this section, we present an overview of the calculation process used in the SPH simulation. First, the initial state is determined for an arbitrary number of particles with uniform displacement. Subsequently, a list of neighbor particle pairs is created to speed up the search of interacting particle pairs that are placed within the smoothing length. Then, the right-hand side of Eq. (3) is calculated

using the pair list to update particle velocities, and particle positions are also updated using updated velocities according to Euler's method. Finally, density is calculated from updated velocity according to Eq. (4), and local pressure is calculated from updated density using Eq. (5).

Computational conditions for dam-break simulation

Table 1 lists the parameters used in the SPH simulation for generating tsunami-like waves. This simulation employed a dam-break system for generating tsunami-like waves and was carried out in 2D because the fluid motion in the depth direction across the wave propagating direction was negligibly small. The initial water mass was held in a reservoir with a length of 50 m and a depth of d_0. The spatial resolution of the computation was set to 0.005 m as the SPH particle size, and the smoothing length l was chosen to be 2.1 times larger than the particle size to solve wave propagation with sufficient accuracy. In this setup, depending on the water depth, the number of SPH particles in the water mass can reach two million, which makes the cost of computation very high. Therefore, we used highly effective parallel computing techniques (Furuichi and Nishiura, 2017) to simulate wave propagation on a long-term scale of 40 s and employed a long channel length of 64 m. As a result, the computational time could be reduced to ~12 h by using 96 central processing unit nodes of the K computer (RIKEN).

Table 1. SPH simulation conditions.

Parameter	Value
Density ρ_0	1000 kg/m^3
Kinematic viscosity ν^K	1 μm^2/s
Speed of sound c_0	125 m/s
Smoothing length l	0.0105 m
Impoundment depth d_0	0.4 m, 0.63 m, 0.82 m
Initial water depth h_0	0 m (dry bed), 0.05 m (wet bed)
Channel length	14 m (length of water mass is 50 m)

EXPERIMENTAL METHODOLOGY

Wave generation

All experimental tests were performed in a large-scale facility at LCH-EPFL. Waves were generated by vertical release of water from an upper reservoir with a storage volume of 7 m^3. Gate opening induced a sudden water level difference between upstream and downstream reservoirs, resulting in gravitational flow into the channel (Fig. 1). These waves propagated into a horizontal channel with a length of 15.5 m and a width of 1.4 m. The channel was smooth, with the Darcy-Weisbach friction factor f approximately equaling 0.02. Specific details of the wave generation technique can be found in the work of Wüthrich (2018).

The use of three independent gates (Wüthrich et al. 2018) allowed one to control the initial discharge Q_0 and generate waves with different hydrodynamic properties. The system also allowed one to generated surges on an initially dry bed and bores propagating on a still water level h_0. In the case of tsunamis, a dry bed surge would represent the first incoming wave, whereas a wet bed bore would represent any additional wave.

Instrumentation

Propagating waves were investigated in terms of flow depths using 7 USs (Baumer UNAM 30I6103) with a precision of ± 0.5 mm and a frequency of 12.5 Hz. These sensors were installed at distances of x = 2, 10.10, 12.10, 13.10, 13.35, 13.60, and 13.85 m from the channel inlet. A higher US concentration between 13.10 m < x < 13.85 m allowed for a more precise investigation of the wave tip shape (Fig. 1).

In-wave velocity profiles were measured using a UVP produced by Metflow (Switzerland). This instrument allowed one to detect instantaneous velocity profiles by making use of the Doppler effect (Meile et al. 2007, Birkhofer et al. 2016). An emitting frequency of 2 MHz was chosen, and the probe was installed in the channel bottom at x = 13.85 m with a vertical inclination of 20° in the upstream direction (Fig. 1). Sensitivity analysis determined the optimum number of repetitions per measurement as 128, and acquisition frequencies of 12–55 Hz were consequently employed (Wüthrich et al. 2016b). Hydrogen bubbles produced by electrolysis were used to increase the acoustic scattering of the flow (Blankaert and Lemmin, 2006; Meile et al., 2011). The synchronization of all instruments was achieved using a LabView® data acquisition system including a transistor-transistor logic level (+5 V, min) trigger signal connected to the UVP probe.

Analogy with dam-break waves

In view of their long periods and wavelengths, dam break-waves are widely accepted to reproduce tsunami-like waves (Chanson, 2006; Nistor et al., 2009). Wüthrich et al. (2018) showed that the vertical release technique generates waves similar to those observed in the classical dam-break scenario. Similar vertical release techniques were previously used by Chanson et al. (2002), Rossetto et al. (2011), Lukkunaprasit et al. (2009), Meile et al. (2011), and Foster et al. (2017). As detailed by Wüthrich et al. (2018), the propagating dry bed surges and wet bed bores generated employing the vertical release technique were in good agreement with the theoretical predictions of Ritter (1892) and Stoker (1957), respectively. In addition, the initial discharge through pipes (Q_0) generated constant water depths in the initial side of the channel (x = 0 m). Similarly to what was discussed by Chanson et al. (2002) and Wüthrich (2018), an equivalent impoundment depth d_0 was derived from the initial discharge Q_0 as

$$d_0 = \frac{9}{4}\left(\frac{Q_0^2}{gW^2}\right)^{1/3}, \quad (8)$$

where g is the gravity constant, and W is the channel width. Based on this equation, the values of d_0 were calculated as 0.40, 0.63, and 0.82 m (Table 2).

Table 2. Test conditions used for numerical model validation. Unit: (m)

Test no.	1	2	3	4	5	6
Bed condition	Dry	Dry	Dry	Wet	Wet	Wet
Initial water depth	0.00	0.00	0.00	0.05	0.05	0.05
Impoundment depth	0.40	0.63	0.82	0.40	0.63	0.82

TEST CONDITIONS

Tests were carried out for three different released discharges under both dry and wet bed conditions (Table 2).

RESULTS AND DISCUSSION

In this section, the main characteristics of dry bed surges and wet bed bores obtained experimentally through vertical release and dam-break simulation are compared and discussed. For both surges and bores, water surface profiles along the longitudinal axis of the wave channel, wave front celerities, and wave velocity profiles along the vertical direction at US7 (Fig. 1) were investigated.

Dry bed surges

The water wave propagation of the surge on a dry smooth channel visually appeared as a thin water layer followed by a continuous rise in water depth until a maximum value was reached. Subsequently, the wave height started to decrease. The wave front propagated uniformly,

and no aeration was observed in the wave front region, as shown in Fig. 3(b). Good agreement was observed between the characteristics of simulated (Fig. 3(a)) and experimental (Fig. 3(b)) propagating wave shapes. In the following sections, the main characteristics of dry bed surges such as wave height profile, wave front celerity, and wave velocity profile are discussed in detail.

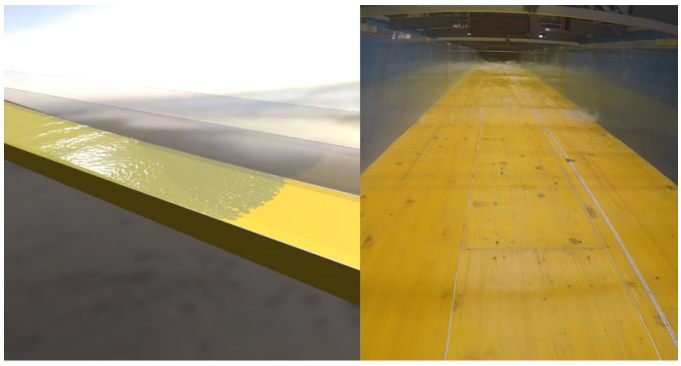

(a) Simulation (b) Experiment

Fig. 3 Wave front shapes of the surge propagating over a dry bed obtained for (a) a dam-break simulation and (b) a vertical release experiment.

Longitudinal water surface profile. Experimentally, the longitudinal water surface profiles were captured for multiple dry bed surges under identical initial release conditions when the surge reached the location of x = 13.85 m (US7). These profiles were compared with numerical simulation data and the theoretical parabolic profile of Ritter (1892) given by

$$\frac{h}{d_0} = \frac{1}{9}\left(2 - \frac{x}{t\sqrt{g d_0}}\right)^2, \tag{9}$$

where h is the local wave height at location x and time t.
Figure 4 shows the results obtained for each impoundment depth d_0, revealing that the wave height featured minor dispersion due to water surface fluctuations, especially for the case of d_0 = 0.82 m. Nevertheless, all experimental tests could well reproduce the theoretical solution. On the other hand, numerical simulations only qualitatively reproduced experimental data in all test cases, and some differences were found in the front part of the surge. In particular, simulation results were in good agreement with experiment and theory in the case of d_0 = 0.63 m, as shown in Fig. 4(b). However, in case of d_0 = 0.40 m, the longitudinal wave profile was a little higher, and the wave front shape was steeper compared to experimental and theoretical (Ritter) results. Because the wave front shape rapidly becomes thinner as the wave propagates under the dry bed condition, the number of SPH particles existing in the wave front decreases, i.e., the spatial resolution of computation is insufficient. Therefore, the error of simulation was assumed to be caused by the influence of numerical dissipation due to the lack of spatial resolution. On the contrary, for the case of d_0 = 0.82 m, the simulated wave height was slightly lower and the wave front steepness was milder than in the experimental case. Notably, although the wave front shape and velocity observed experimentally may be influenced by small roughnesses on the channel floor (Wüthrich, 2018), the simulation boundary conditions assumed a completely smooth channel floor and a non-slip condition. Therefore, the agreement between experiment and simulation may be improved if the effects of roughness are considered. However, the use of small SPH particle size makes it difficult to directly resolve roughness on the floor, since the computational cost in this case is too high to solve the actual phenomena observed in the experiment. Therefore, a new boundary model to reproduce the effect of surface roughness is currently under development.

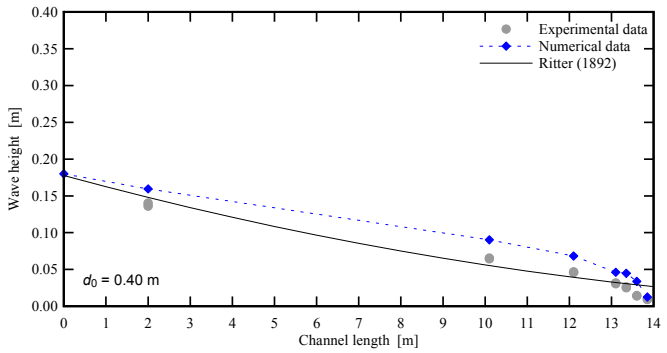

(a) Test 1

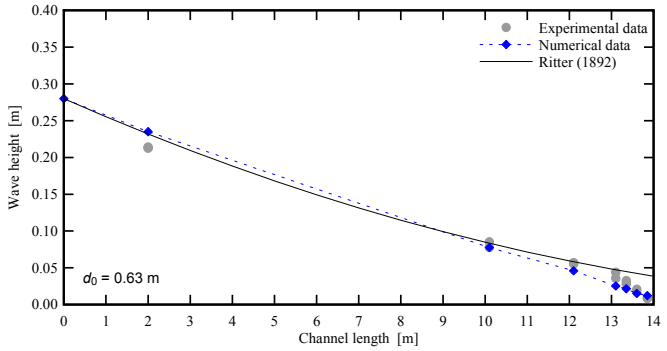

(b) Test 2

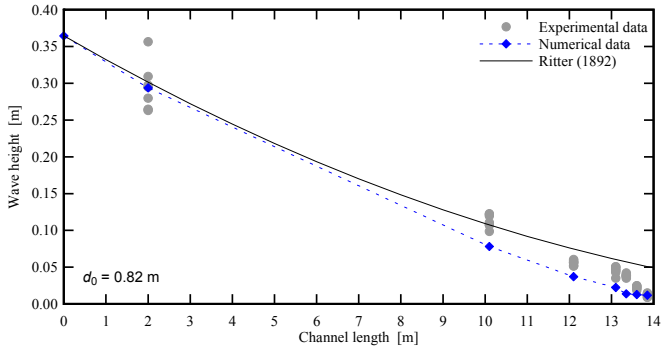

(c) Test 3

Fig. 4 Longitudinal water surface profiles of dry bed surges obtained by experiment and simulation when the wave front reached the measurement location at x = 13.85 m of US7. Comparison of water surface profiles of surges obtained for d_0 = (a) 0.40 m, (b) 0.63 m, and (c) 0.82 m with the theoretical solutions of Ritter (1892).

Wave front celerity. Wave front celerity values were derived from the spatiotemporal advancement of the wave front. The average front celerity of the propagating wave (U) was estimated as

$$U = \frac{\Delta x}{\Delta t}, \tag{10}$$

where Δx is the distance between two different measurement points,

and Δt is the difference of the wave front arrival time for these points. The average front celerity was considered for x = 10.10, 12.10, 13.10, 13.35, 13.60, and 13.85 m relative to the point of x = 2.0 m from the channel inlet. Figure 5 compares the average front celerities obtained by SPH simulation for dry bed surges to values obtained using formulae that are commonly employed in design codes and practice and are mostly derived from laboratory-scale physical models. This comparison proved that wave front celerities obtained by numerical simulation were consistent with values obtained by other wave generation mechanisms described in literature. Although the celerity range described in literature is wide, the simulated values were roughly positioned in the center of this range and were relatively close to values predicted using the formula of Wüthrich et al. (2018). This finding shows that simulated celerities were within the acceptable range of experimental values. Therefore, we confirmed that SPH simulation can reproduce tsunami-like waves with high reliability for the dry bed condition and can consequently predict wave front celerities with high precision.

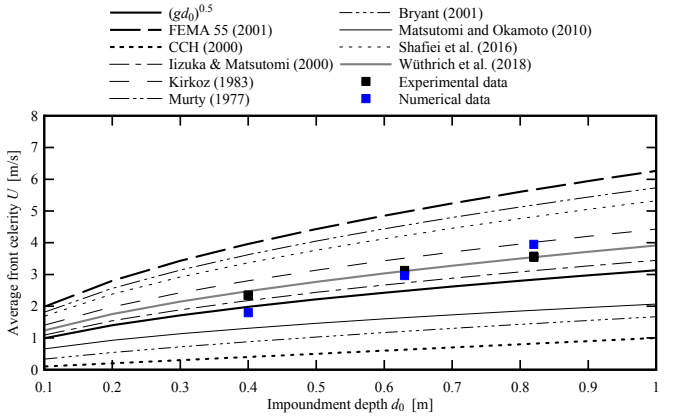

Fig. 5 Comparison of average front celerities obtained by SPH simulation for dry bed surges with values obtained using formulae reported in literature.

Wave velocity profile. Under experimental conditions, the internal instantaneous velocity profiles of propagating waves can be measured using a UVP probe installed in the channel bottom at x = 13.85 m from the channel inlet, similarly to the method described by Meile et al. (2011). A representative velocity profile for a dry bed surge with d_0 = 0.82 m is shown in Fig. 6, which presents typical profiles associated with turbulent open-channel flows. Note that this wave profile was obtained at a "quasi" steady state when the wave was sufficiently well developed. In the experiment, a well-defined boundary layer was observed to the height of 0.05 m from the bottom of channel, which was followed by an upper region with almost constant velocities. The boundary layer was also observed in the simulation; however, the thickness of the simulated boundary layer exceeded that observed experimentally. In addition, simulated wave velocity was 1.5 times higher than the experimental value. These findings were ascribed to the fact that the spatial resolution of computation might be not sufficient to reproduce the thin boundary layer, since the thickness of the boundary layer estimated by the experiment had a size corresponding to only 10 particles in the SPH simulation. Although much higher resolution is necessary for precise computation, it is not practical to reproduce tsunami-like waves by such high-resolution simulation because of high computational costs, which is the limitation of the present simulation.

Wet bed bores

Figures 7(a) and (b) show snapshots of simulated and experimental water wave propagation of the bore on the wet channel, respectively. Differences between the wave propagation patterns of dry bed surges and wet bed bores are clearly highlighted by comparison of Fig. 3 with Fig. 7. In the experiment, the propagating bore was visually similar to a propagating hydraulic jump. Significant air entrainment in water was observed behind the bore front, where air bubbles could be detected. In contrast, mainly clear water was observed farther behind the front, in agreement with the previous findings of Leng and Chanson (2015).

The shape of the simulated bore front (Fig. 7(a)) was steeper than that observed for the dry bed surge, in agreement with experiments and previous literature. Visually, we could confirm that the shape of the propagating wave was in very good agreement with the experiment. However, air entrainment within the wave front could not be observed, because the air flow was not calculated in the SPH simulation, as described in the above section. The influence of aeration on the main wave characteristics is also discussed in the following sections, where the main characteristics of wet bed bores such as longitudinal water surface profile, wave front celerity, and wave velocity profile are compared with experimental results in detail.

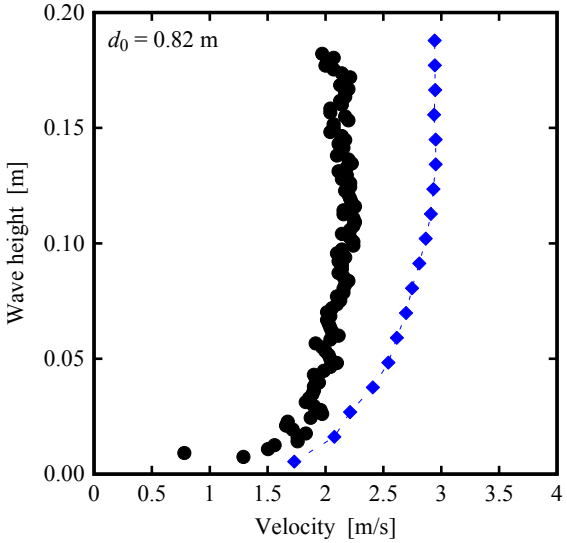

Fig. 6 Fluid velocity distribution in the wave height direction at time t = 9.1 s for a dry bed surge with d_0 = 0.82 m of Test 3, measured at x = 13.85 m from the channel inlet. Black circles and blue diamonds represent experimental and simulation data, respectively.

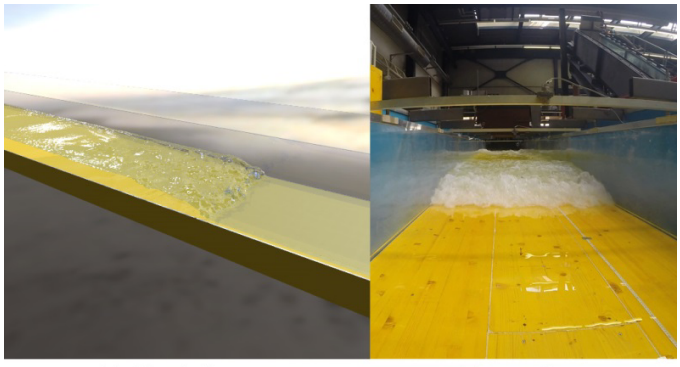

(a) Simulation (b) Experiment

Fig. 7 Wave front shapes of a bore propagating over a wet bed obtained by (a) dam-break simulation and (b) vertical release experiment with an initial still water depth of 0.05 m.

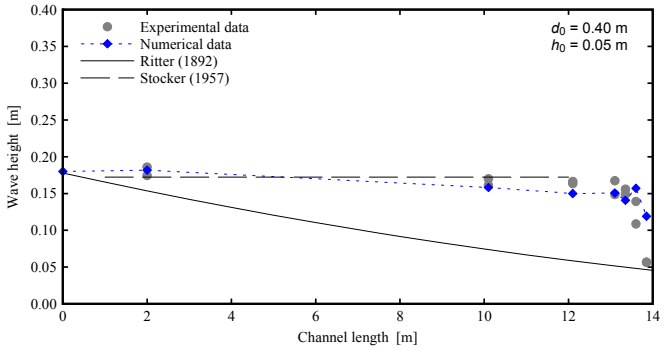

(a) Test 4

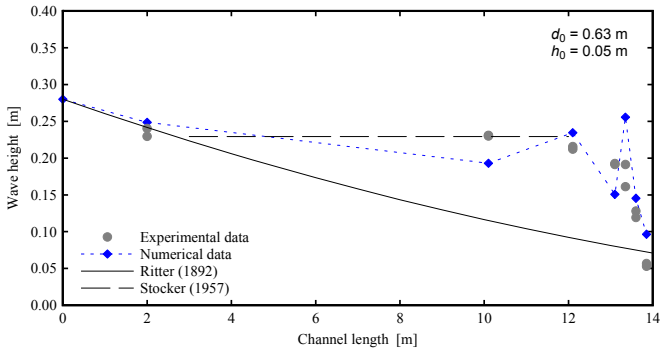

(b) Test 5

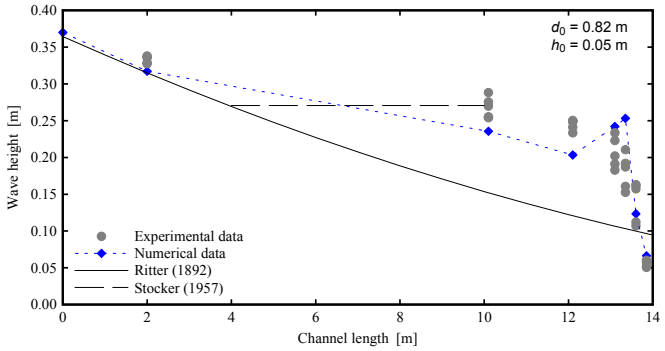

(c) Test 6

Fig. 8 Longitudinal water surface profiles of wet bed bores obtained by experiment and simulation when the wave front reached the measurement location at x = 13.85 m (US7). Comparison of water surface profiles of bores obtained for d_0 = (a) 0.40 m, (b) 0.63 m, and (c) 0.82 m with the theoretical solutions of Ritter (1892) and Stoker (1957). The initial water depth was set to 0.05 m.

Longitudinal water surface profile. According to Stoker (1957), for a wave longitudinal profile of a dam-break bore propagating over a wet bed, temporal wave evolution can be divided into four main regions from downstream to upstream, namely (1) a turbulent bore front; (2) a plateau, i.e., a region with almost constant water height h_2 (horizontal dashed line in Figure 8); (3) a far back region where the Ritter (1892) theory can be applied; and (4) an upstream reservoir where h is equal to d_0.

Figure 8 shows experimental and simulated longitudinal profiles of the water surface for each impoundment depth captured when the wave front arrived at the location of x = 13.85 m from the channel inlet. Note that the wave front arrival time was defined as the time when a threshold of wave height h was registered to h_0 + 0.01 m. These profiles were also compared with those of Ritter (1892) in the far back region and with those of Stoker (1957) in the plateau region with almost constant water height h_2. The experimental profiles were in good agreement with theoretical solutions in all test cases, which confirmed that the vertical release technique can produce bores comparable to those generated in a classical dam-break scenario.

On the other hand, although the simulation could relatively well reproduce experimental profiles and theoretical solutions, the simulated wave height was slightly lower than experimental and theoretical values in the plateau region near the wave front, especially for d_0 = 0.82. With increasing impoundment depth, the turbulent flow becomes significant and causes air entrainment in the wave front. Therefore, our simulation may underestimate the influence of turbulence with aeration on the wave height, because SPH does not account for air flow. If aeration is considered in the simulation, its results may be improved. However, multiphase flow simulation of water and air by SPH is very difficult, because the air-water density difference is too large for stable-state fluid flow calculations. Nevertheless, for the tested impoundment depths, it was shown that simulation was able to reproduce the wave height from downstream to upstream and the front shape of bores propagating over the wet bed in acceptable quality.

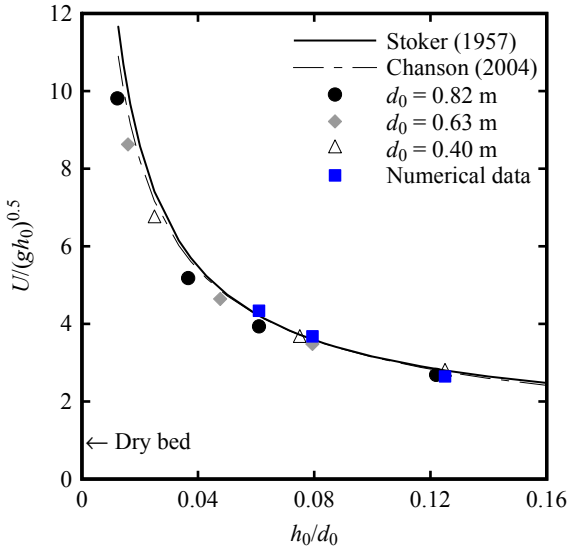

Fig. 9 Average front celerity of bores as a function of initial still water depth h_0. Blue squares represent simulation data, and other symbols represent experimental data. Simulation data were compared not only with experimental data but also with both the theoretical solution of Eq. (11) presented by Stoker (1957) and the empirical approximation proposed by Chanson (2004). In the experiment, initial still water depths of 0.01, 0.03, 0.05, and 0.1 m were used for each impoundment depth. In the simulation, the initial still water depth was fixed at 0.05 m for each impoundment depth.

Wave front celerity. Under identical discharge conditions, wet bed bores propagate with a slower front celerity than dry bed surges. The front celerity U of a bore propagating over a wet bed can be expressed as a function of the initial still water depth h_0. The front celerity values for decreased h_0 reached those observed for the dry bed condition. Figure 9 compares the wave front celerity U with values calculated using a theoretical solution derived from Eq. (11), presented by Stoker (1957), and with the empirical approximation of Montes (1998) in Eq. (12), presented by Chanson (2004).

$$\frac{U}{\sqrt{gh_0}} = \sqrt{\frac{1}{8}\cdot\left[\left(2\cdot\frac{h_2}{h_0}+1\right)^2-1\right]}, \quad (11)$$

$$\frac{U}{\sqrt{gh_0}} = \frac{0.63545+0.3286(h_0/d_0)^{0.65167}}{0.00251+(h_0/d_0)^{0.65167}}. \quad (12)$$

Both experimental and simulation results showed very good agreement with all formulae. Therefore, contrary to the case of dry bed surges, the front celerity for wet bed bores can be precisely predicted by our simulation method, since the influence of bed roughness in the presence of initial still water on the floor is negligible.

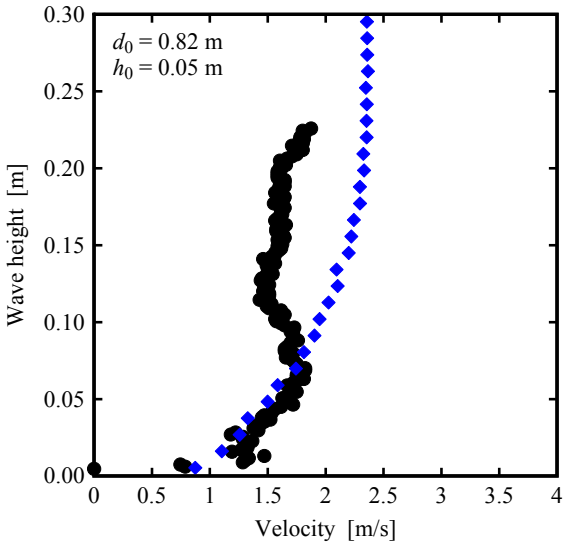

Fig. 10 Fluid velocity distribution in the wave height direction at time t = 9.6 s for a wet bed bore with an initial still water depth h_0 = 0.05 m and an impoundment depth d_0 = 0.82 m of Test 6, measured at x = 13.85 m from the channel inlet. Black circles and blue diamonds represent experimental and simulation data, respectively.

Wave velocity profile. Figure 10 shows a representative velocity profile for a wet bed bore with an initial still water depth of 0.05 m at d_0 = 0.82 m. This profile was measured at x = 13.85 m from the channel inlet when the wave was sufficiently well developed to the steady state. Numerical simulation confirmed that bores moved slower than dry bed surges (Fig. 6) and was found to well reproduce experimental velocity profiles within the wave height of 0.07 m from the channel bottom. In the upper region of the wave (from the wave height of 0.07 m to 0.1 m), the experimental velocity decreased and then became constant, while the simulated velocity did not decrease and stayed constant. Experimental observations indicated that the entrainment of air bubbles in the wave could reduce measurement precision by UVP. In addition, Yeh and Mok (1990) mentioned that flow separation initiated at the front toe resulting from streamline divergence caused by the sudden raise in water depth results in the formation of a wave front roller. These air bubbles and eddies arising in the wave front might influence the flow velocity profile behind the wave front. However, the authors believe that these effects cannot be sufficiently estimated by the simulation because of the limitation of the simulation model without air bubble calculation. Moreover, the spatial resolution of the computation might still be insufficient to resolve such eddies even though the eddy viscous stress is considered by the LES model. The reproducibility of wave profile simulation can be improved by tuning the parameter C_s of Eq. (6) and increasing the resolution, which, however, does not resolve the problem of air bubbles.

CONCLUSIONS

Herein, the reliability of a simulation model for investigating tsunami-like wave propagation under both dry and wet bed conditions was validated by comparison with the results of large-scale experiments and some theoretical solutions. This comparison deepened the understanding of physical phenomenon modeling based on a hybrid experimental-numerical approach for the design of safer infrastructures against tsunami. The simulation model was developed by JAMSTEC and employed the SPH method involving a highly efficient parallel computing technique to simulate large-scale tsunami-like waves with increased precision. During the development of experimentally validated numerical tools for a better understanding of tsunami-like flows, the following preliminary results on the reproducibility and current limitations of the simulation were obtained:

- For the dry bed surge, the best agreement of the wave height profile with experiment and theory was found for d_0 = 0.63 m. Although the simulation qualitatively reproduced the wave height profile in all test cases, slight deviations from experimental observations were observed in terms of wave front steepness. In addition, observations of the wave velocity profile implied that although the simulation reproduced the boundary layer, the thickness of the boundary layer and the wave velocity of the upper layer were slightly overestimated. These discrepancies were ascribed to the insufficient spatial resolution of the computation and the ignorance of channel floor roughness. Further, the simulation precisely predicted wave front celerity values, which were consistent with those obtained using other wave generation mechanisms described in literature.
- For the wet bed bore, the simulation reproduced the wave front shape and the wave height profile from downstream to upstream in acceptable quality. However, for d_0 = 0.82 m, the wave profile was slightly underestimated in the plateau region near the wave front. Moreover, although the simulation well reproduced the experimental velocity profile within the lower region of the wave, a large velocity difference was found in the upper wave region. Contrary to the case of dry bed surges, significant entrainment of air bubbles and eddy flows were experimentally observed for wet bed bores, becoming more significant with increasing impoundment depth. However, the effect of air bubbles could not be considered numerically, because the simulation did not account for air flow. In addition, the spatial resolution of the computation might be insufficient to resolve such eddies, even though the eddy viscous stress was considered by the LES model. On the other hand, the wave front celerity was precisely predicted by the simulation method, because the influence of channel floor roughness in the presence of a sufficient amount of initial still water on the floor is negligible.

As a result, it was confirmed that the employed model can well reproduce wave front celerity under both dry and wet bed conditions. However, this model can be further improved to quantitatively reproduce the wave profiles of height and velocity. In the future, it is planned to investigate the effects of spatial resolution and LES model parameters to mitigate the above problems and ensure simulation reproducibility. Moreover, the development of a boundary layer model considering channel floor roughness is currently undergoing.

ACKNOWLEDGEMENTS

This study was supported by the Earth Simulator project of JAMSTEC, MEXT as “Priority Issue on Post-K computer” (System for Integrated Simulation of Earthquake and Tsunami Hazard and Disaster) using

computational resources of the K computer provided by the RIKEN Center for Computational Science through the HPCI System Research project (Project ID: hp180207, "Joint Usage/Research Center for Interdisciplinary Large-scale Information Infrastructures" and "High Performance Computing Infrastructure" in Japan (Project ID: jh180060-NAH, jh180065-NAH), and the Swiss National Science Foundation (SNSF) (Grants 200021_149112/1 and 200021_149112/2).

REFERENCES

Birkhofer, B, Meile, T, De Cesare, G, Jeelani, SAK and Windhab, EJ (2016). "Use of gas bubbles for ultrasound Doppler flow velocity profile measurement," *Flow Meas. Instrum.*, 52, 233–239.

Blankaert, K, and Lemmin, U (2006). "Means of noise reduction in acoustic turbulence measurements," *J. Hydraul. Res*., 44(1), 3–17.

Bryant, E (2001). *Tsunami: The underrated hazard, 1st Ed.*, Cambridge University Press.

CCH (2000). *City and County of Honolulu Building Code (CCH)*, Department of Planning and Engineering of Honolulu Hawaii.

Chanson, H (2004). *The hydraulics of open channel flow: An introduction, 2nd Ed.*, Elsevier.

Chanson, H. (2006). "Tsunami surges on dry coastal plains: Application of dam break wave equations," *Coastal Eng. J.*, 48(4), 355–370.

Chanson, H, Aoki, S, and Maruyama, M (2002). "Unsteady air bubble entrainment and detrainment at a plunging breaker: Dominant time scales and similarity of water level variations," *Coastal Eng*., 46(2), 139–157.

Crespo, AJ, Dominguez, JM, Rogers, BD, Gomez-Gesteira, M, Longshaw, S, Canelas, R, Vacondio, R, Barreiro, A, and Garcia-Feal, O (2015). "DualSPHysics: Open-source parallel CFD solver based on Smoothed Particle Hydrodynamics (SPH)," *Comput. Phys. Comm.*, 187, 204–216.

FEMA (2001). *Coastal construction manual: Principles and practices of planning, siting, designing, constructing, and maintaining residential buildings in coastal regions*, DIANE Publishing.

Foster, ASJ, Rossetto, T, and Allsop, W (2017). "An Experimentally Validated Approach for Evaluating Tsunami Inundation Forces on Rectangular Buildings," *Coastal Eng*., 128, 44–57.

Furuichi, M, and Nishiura, D (2017). "Iterative Load-Balancing Method with Multigrid Level Relaxation for Particle Simulation with Short-Range Interactions," *Comput. Phys. Comm.*, 219, 135–148.

Guler, HG, Baykal, C, Arikawa, T, and Yalciner, AC (2018). "Numerical assessment of tsunami attack on a rubble mound breakwater using OpenFOAM (R)," *Appl. Ocean Res.*, 72, 76–91.

Iizuka, H, and Matsutomi, H (2000). "Damage due to flood flow of tsunami," *Proc. Coastal Eng. JSCE*, 47, 381–385.

Kirkoz, M (1983). "Breaking and run-up of long waves, tsunamis: Their science and engineering," *Proc. 10th IUGG Int. Tsunami Symp.*, Terra Scientific.

Lauber, G, and Hager, WH (1998). "Experiments to Dambreak Wave: Horizontal Channel," *J. Hydraul. Res*, 36(3), 291–307.

Leng, X, and Chanson, H (2015). "Breaking bore: Physical observations of roller characteristics," *Mech. Res. Commun.*, 65, 24–29.

Lukkunaprasit, P, Thanasisathit, N, and Yeh, H (2009). "Experimental verification of FEMA P646 tsunami loading," *Journal of Disaster Research*, 4(6):410–418.

Matsutomi, H, and Okamoto, K (2010). "Inundation flow velocity of tsunami on land," *Isl. Arc*, 19(3), 443–457.

Meile, T, De Cesare, G, Blanckaert, K and Schleiss, AJ (2007). "Improvement of Acoustic Doppler Velocimetry in steady and unsteady turbulent open-channel flows by means of seeding with hydrogen bubbles," *Flow Meas. Instrum.*, 19, 215–221.

Meile, T, Boillat, J-L, and Schleiss, AJ (2011). "Water-surface oscillations in channels with axi-symmetric cavities," *J. Hydraul. Res*., 49(1), 73–81.

Monaghan, JJ (1992). "Smoothed Particle Hydrodynamics," *Annu. Rev. Astron. Astrophys.*, 30, 543–574.

Monaghan, JJ (1994). "Simulating Free Surface Flows with SPH," *J. Comput. Phys.*, 110 (2), 399–406.

Montes, S (1998). *Hydraulics of open channel flow*, ASCE.

Murty, TS (1977). *Seismic sea waves: Tsunamis*, Dept. of Fisheries and the Environment Fisheries and Marine Service.

Nishiura, D, Furuichi, M, and Sakaguchi, H (2015). "Computational Performance of a Smoothed Particle Hydrodynamics Simulation for Shared-Memory Parallel Computing," *Comput. Phys. Comm.*, 194, 18–32.

Nistor, I, Palermo, D, Nouri, Y, Murty, T, and Saatcioglu, M (2009). *Handbook of Coastal and Ocean Engineering*, World Scientific, 261–286.

Nouri, Y, Nistor, I, Palermo, D, and Cornett, A (2010). "Experimental Investigation of the Tsunami Impact on Free Standing Structures," *Coastal Eng. J.*, 52(1), 43–70.

Ramsden, JD (1993). "Tsunami: Forces on a Vertical Wall Caused by Long Waves, Bores, and Surges on a Dry Bed," *Ph.D. thesis*, California Institute of Technology, Pasadena, CA.

Ritter, A (1892). "Die Fortpflanzung der Wasserwellen," *Zeitschrift des Vereins Deutscher Ingenieure*, 36, 947–954.

Rossetto, T, Allsop, W, Charvet, I, and Robinson, D (2011). "Physical modelling of tsunami using a new pneumatic wave generator," *Coastal Eng.*, 58(6), 517–527.

Shafiei, S, Melville, BW, and Shamseldin, AY (2016). "Experimental investigation of tsunami bore impact force and pressure on a square prism," *Coastal Eng.*, 110, 1–16.

St-Germain, P, Nistor, I, Townsend, R, and Shibayama, T (2014). "Smoothed-Particle Hydrodynamics Numerical Modeling of Structures Impacted by Tsunami Bores," *J. Waterway, Port, Coastal, Ocean Eng.*, 140(1), 66–81.

Stoker, JJ (1957). *Water waves: The mathematical theory with applications*, John Wiley& Sons.

Wüthrich, D., Pfister, M, Manso, P, Constantinescu, G. and Schleiss, AJ (2016a). "Surface Turbulence on Bores and Surges propagating on smooth and rough beds," *Proc. of the 6th International Conference on the Application of Physical Modelling in Coastal and Port Engineering and Science* (Coastlab16), May 10-13, Ottawa, Canada.

Wüthrich, D., Pfister, M, De Cesare, G, and Schleiss, AJ (2016b). "Velocity profile measurements in bore waves," *Proc. of the 10th International Symposium on Ultrasonic Doppler Methods for Fluid Mechanics and Fluid Engineering* (10th ISUD), September 28-30, Tokyo, Japan, pp. 137-140

Wüthrich, D, Pfister, M, Nistor, I, and Schleiss, AJ (2018). "Experimental Study of Tsunami-Like Waves Generated with a Vertical Release Technique on Dry and Wet Beds," *J. Waterway, Port, Coastal, Ocean Eng.*, 144(4), 04018006.

Wüthrich, D (2018). "Extreme Hydrodynamic impact onto buildings," *EPFL PhD Thesis (N. 8116)*, Lausanne, Switzerland, 264 pages.

Yeh, HH, and Mok, K-M (1990). "On turbulence in bores," *Phys. Fluids A*, 2(5), 821–828.